Macromolecules
ARTICLE

Macromolecules **2010**, *43*, 1981–1991 **1981**
DOI: 10.1021/ma9026096

Hydrogen-Bond Engineering in Supramolecular Polymers: Polarity Influence on the Self-Assembly of Benzene-1,3,5-tricarboxamides

Tristan Mes, Maarten M. J. Smulders, Anja R. A. Palmans,* and E. W. Meijer*

Laboratory of Molecular Science and Technology, Eindhoven University of Technology, P.O Box 513, NL-5600 MB Eindhoven, The Netherlands

Received November 26, 2009; Revised Manuscript Received January 15, 2010

ABSTRACT: Benzene-1,3,5-tricarboxamides (BTAs) comprising alkyl side chains form supramolecular polymers in dilute solution and in the solid state as a result of the 3-fold helical arrangement of the intermolecular hydrogen bonds. We investigated systematically the role of polarity on the self-assembling behavior of BTAs in dilute solution and, when incorporated in polymeric materials, on their ability to phase segregate. In dilute solutions, the polarity was gradually increased by mixing in methyl *tert*-butyl ether (in which BTAs are molecularly dissolved) into methylcyclohexane (in which BTAs form stable helical aggregates). We observed a significant decrease in the stability of BTA aggregates after the addition of small amounts of ether. This strong dependence on the polarity of the environment was also found in the solid state. By end-capping telechelics of varying polarity with the BTA motif, a wide range of backbone polarities was covered. Commercially available polymers as well as polymers that were synthesized via ring-opening metathesis polymerization were evaluated. BTA motifs connected to apolar telechelics formed stable phase segregated nanorods. Increasing the polarity resulted in a decrease of the stability, and this eventually resulted in the loss of nanorod formation. This systematic study on the influence of polarity on self-assembly gives us a detailed understanding of the potential to use BTAs as functional nanorods in various applications.

Introduction

The field of supramolecular polymeric materials has grown rapidly over the past decade.[1−9] The potential of supramolecular polymers arises from their tunable thermal and mechanical properties, combined with a highly dynamic and reversible character.[10−13] This facilitates processing and gives rise to new and unique material properties with applications envisioned in biomaterials,[14−16] self-healing materials,[17−20] hydrogels[21,22] and optoelectronic devices.[23−25] The noncovalent interactions that are responsible for the reversible bonds can be based on hydrogen bonding, $\pi-\pi$ interactions, dipole interactions, metal−ligand complexation, hydrophobic or solvophobic interactions, and combinations thereof. A particularly interesting class of supramolecular polymers is that of polymer chains based on low molar mass monomers end-capped with multiple hydrogen-bonding units.[11,26−35] Under suitable conditions, these supramolecular polymers display macroscopic material properties comparable to high molecular weight macromolecules. Besides the strength of the noncovalent interaction, also the propensity to phase-segregate was found to be important for the polymer properties.[8,36] This phase segregation results in strong multiple physical cross-linking points in two or three dimensions within the soft polymer matrix, which eventually can result in thermoplastic elastomeric properties.[36] In the past, our group has successfully employed the quadruple hydrogen-bonding ureidopyrimidinone (UPy) unit for this purpose. It was observed that thermoplastic elastomeric properties were only obtained when additional lateral interactions were present next to the dimerization of the UPys by hydrogen bonding since they ensured the formation of columnar structures, resulting in phase segregation between the hard rods and the soft polymer.[12,37]

*Corresponding authors. E-mail: E.W.Meijer@tue.nl (E.W.M.), A.Palmans@tue.nl (A.R.A.P.).

We recently showed the presence of 1D columnar structures in telechelic poly(ethylene butylene) (pEB) functionalized with the benzene-1,3,5-tricarboxamide (BTA) motif.[38] BTAs have been studied in detail as liquid crystals, organogelators, and nucleating agents for poly(propylene).[39−45] A 3-fold helical arrangement of the intermolecular hydrogen bonds stabilizes the columnar packing of the BTA disks in the solid state and in dilute heptane solution.[46,47] Circular dichroism (CD) spectroscopy showed that the introduction of homochiral side chains results in columnar structures with a preferred helicity.[48] BTA motifs end-capped or copolymerized with pEB induced physical cross-linking via the formation of nanorods in solution and in the solid state as evidenced by UV, CD, and IR spectroscopy.[38] A distinct fibrillar structure was observed with atomic force microscopy (AFM) which is indicative for phase segregation between the PEB soft phase and the BTA columnar aggregates. This intrinsic phase segregation of BTA nanorods with an amorphous polymer resulted in thermoplastic elastomeric behavior.

In solution, self-assembly based on hydrogen bonding is highly affected by the choice of solvent. Typically, low-polarity solvents are used to enhance the formation of hydrogen bonds, or alternatively, a hydrophobic shell is introduced to shield the hydrogen bonds from its polar environment.[49,50] While BTAs form helical stacks in dilute solutions of apolar alkane solvents as a result of a high association constant (3×10^7 M^{-1}), the intermolecular hydrogen bonds disappear in more polar solvents like chloroform or methanol.[47,48,51] Moreover, in apolar sovents the propensity to form columnar helical stacks is significantly lowered when changing one alkyl side chain in a BTA to an oligo(ethylene oxide) side chain due to a dramatic reduction of the association constant (20 M^{-1})[51] caused by backfolding of the oligo(ethylene oxide) side chain. This means that the self-assembly of BTAs into helical aggregates depends not only on the solvent polarity but also on the microenvironment of the BTA.

Published on Web 02/01/2010

Scheme 1. Chemical Structures of Model Compound 1 and BTA End-Capped Polymers 4a−g

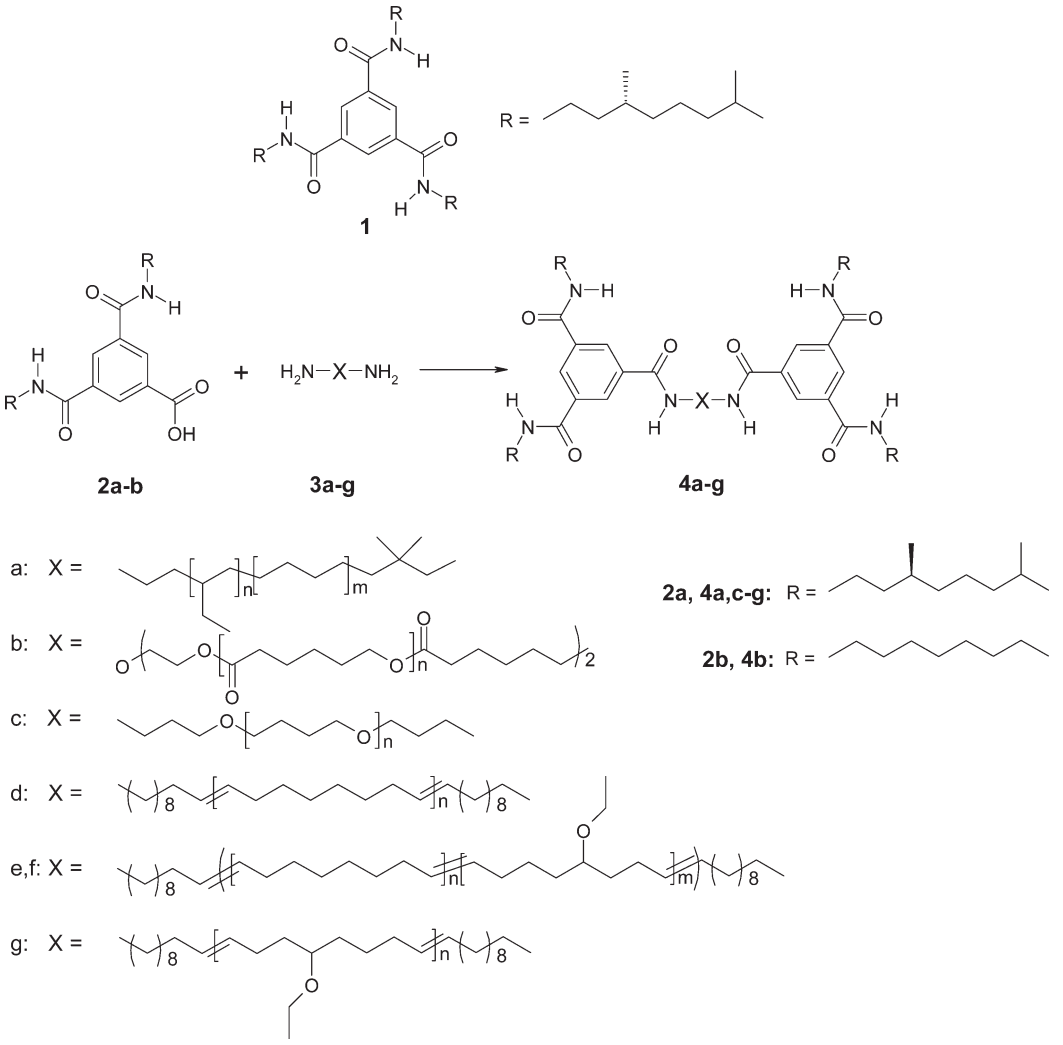

The latter may have a significant impact on the material properties when designing biocompatible and biodegradable polymers end-capped with the BTA unit.

In this paper, we investigate in detail the influence of the environment's polarity on the self-assembly behavior of BTAs in the solid state and in dilute solution. The ability of BTAs to form helical aggregates in dilute solution was taken as an indication for its tendency to phase segregate when incorporated in a polymer matrix. We first performed CD measurements on dilute solutions of BTA **1** (Scheme 1) in alkane/ether mixtures ($c = 10^{-5}$ M), which allows us to investigate systematically the self-assembly of BTAs as a function of solvent polarity. Polarity effects in the solid state, and their influence on BTA nanorod formation, were evaluated by functionalizing telechelic polymers **4a−c** of varying polarity with a BTA precursor. We selected three easily accessible amine-functional telechelics apolar pEB, polar poly-ε-caprolactone (pCL), and medium polar polytetrahydrofuran (pTHF) and subsequently end-capped these polymers with BTA precursor **2** (Scheme 1). In addition, we gradually altered the polymer backbone's polarity by preparing copolymers **4d−g** of cyclooctene (CO) and the more polar 5-ethoxycyclooctene (ECO) via ring-opening methathesis polymerization (ROMP). Cyclooctene-based monomers were selected because of their well-known reactivity in ROMP. We assumed that the difference in ring strain between the two monomers is negligible and therefore leads to random copolymers. The telechelic amine polymers are readily accessible by using a protected amine as a chain transfer agent (CTA) during ROMP. The solid-state properties of these polymers with a varying backbone polarity were investigated with CD spectroscopy, IR spectroscopy, and differential scanning calorimetry (DSC) with the aim to relate backbone polarity to BTA nanorod formation and, ultimately, polymer properties.

Experimental Section

Materials. 3,5-Bis(3*S*)-(3,7-dimethyloctylaminocarbonyl)benzoic acid (**2a**), 3,5-bis(octylaminocarbonyl)benzoic acid (**2b**), *N*,*N*′-(1,20-eicos-10-endiyl)bis(isoindole-1,3-dione) (**7**), bis(3-aminopropyl)poly(tetrahydrofuran) (DSC: T_m = 23 °C, ΔH = 70.69 J/g, M_n = 2800 g/mol, PDI = 1.33) (**3c**), bis(amino)poly(ε-caprolactone) (DSC: T_m = 43 °C, ΔH = 62 J/g, GPC: M_n = 5821 g/mol, PDI = 1.27) (**3b**), and poly(ethylene/butylene)-bisBTA (M_n = 3500 g/mol, PDI = 1.08) (**4a**) were synthesized according to literature procedures.[29,38,52,53] All reagents were purchased from Aldrich or Acros Organics and used as received unless otherwise specified. All solvents were purchased from Biosolve. Dichloromethane and toluene were freshly distilled from sodium before use. THF and chloroform were dried over molecular sieves before use. All ring-opening metathesis polymerizations were performed using the second-generation Grubbs-type initiator, which was purchased from Aldrich. Deuterated solvents were purchased from Cambridge Isotopes Laboratories. All reactions were run in flame-dried glassware under an argon atmosphere.

Instrumentation and Analysis. CD and UV spectra were recorded on a Jasco J-815 CD spectrometer equipped with a

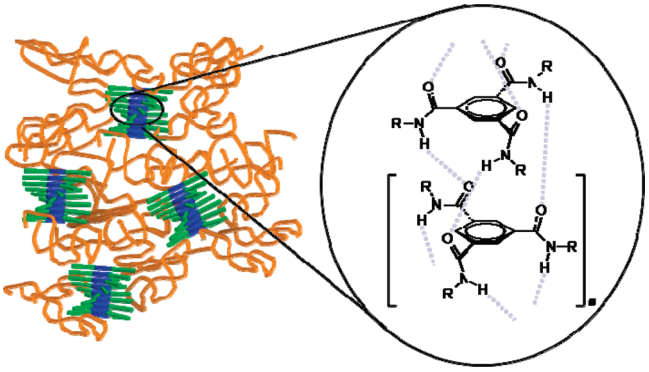

Figure 1. Schematic representation of BTA nanorods embedded in a polymer matrix.

Jasco PTC-348 WI temperature controller. Experiments were conducted using spectroscopic grade methylcyclohexane or methyl *tert*-butyl ether as the solvent. Cells with an optical path length of 1 cm were applied (for $\sim 10^{-5}$ M solutions). The molar ellipticity is calculated as $\Delta\varepsilon$ = CD-effect/(32980*cl*), where *c* is the concentration in mol/L and *l* = the optical path length in cm. Films of **4a**,**c**−**g** were prepared by making solutions of **4a**,**c**−**g** in chloroform (50 mg/mL) and spin-coating a volume of 0.5 mL on 0.40 cm^2 quartz slides at 800 rpm for 2 min. The film thickness was determined with a Tencor P-10 surface profiler. Variable temperature CD measurements on the spin-coated films were performed by mounting the Linkam THMS 600 heating device into the CD apparatus, which allowed heating up to 250 °C. ^{1}H NMR and ^{13}C NMR spectra were recorded on a Varian Gemini 400 MHz NMR (400 MHz for ^{1}H NMR and 100 MHz for ^{13}C NMR). Proton chemical shifts are reported in ppm downfield from tetramethylsilane (TMS). Carbon chemical shifts are reported downfield from TMS using the resonance of the deuterated solvent as the internal standard. IR spectra were recorded on a Perkin-Elmer 1600 FT-IR. Temperature variable IR spectra were recorded on an Excalibur FTS 3000 MX FT-IR from Biorad. GC/MS measurements for performed on a GC-MS QP5000 by Shimadzu equipped with a Phenomenex Zebron ZB-35 column. POM measurements were performed using a Jenaval polarization microscope equipped with a Linkam THMS 600 heating device, with crossed polarizers. The thermal transitions were determined with DSC using a Perkin-Elmer DSC-7 under a nitrogen atmosphere with heating and cooling rates of 40 K/min. GPC measurements were performed on a Resi Pore column with chloroform as the eluent (flow = 1 mL/min) and employing a PDA (λ = 254 nm) as the detector. The molecular weights were determined using the polystyrene calibration method.

Synthesis of BTA-Functionalized Telechelic Polymers. *pCL-bis-BTA* (***4b***). A solution of *N*-(3-(dimethylamino)propyl)-*N*′-ethyl-carbodiimide hydrochloride (EDC) (0.42 mmol, 105 mg) in 2 mL of dry $CHCl_3$ was added to an ice cooled stirred solution of **2b** (0.3 mmol, 127 mg), 4-(dimethylamino)pyridine (DMAP) (0.42 mmol, 51 mg), and **3b** (0.14 mmol, 300 mg) in dry $CHCl_3$ (25 mL). The reaction mixture was allowed to warm to room temperature and stirred overnight. Then the mixture was diluted with $CHCl_3$ (50 mL) and washed successively with HCl (1 M, 50 mL), $NaHCO_3$ (10%, 20 mL), and $NaCl_{aq}$ (saturated, 20 mL). $CHCl_3$ was removed *in vacuo*. The product was precipitated in cold heptane and methanol subsequently and obtained as a white solid. Yield = 170 mg (50%). ^{1}H NMR ($CDCl_3$): δ 8.39 (s, 6H, ArH), 6.61 (t, 2H, NH), 6.51 (t, 4H, NH), 4.23 (t, 4H, $OCH_2CH_2OC{=}O$), 4.06 (t, 2H, $CH_2OC{=}O$), 3.69 (t, 4H, $OCH_2CH_2OC{=}O$) 3.47 (t, 12H, $CONHCH_2$), 2.31 (t, 2H, $OC{=}OCH_2$), 1.8−0.85 (alkyl). ^{13}C NMR ($CDCl_3$): δ 173.8 (C=O), 165.9 (ArC=O), 135.3 (ArC), 127.9 (ArC), 64.4 ($CH_2OC{=}O$), 40.6 (CH_2NH), 34.0, 31.6, 29.1, 28.4, 26.9, 25.7, 24.8, 22.5, 14.3. IR: ν (cm^{-1}): 3333 (N−H stretch), 1664 (amide I), 1541 (amide II). GPC: M_n = 12.4 kg/mol, M_w = 14.2 kg/mol, PDI = 1.15. DSC (40 K/min): T_m = 43 °C, ΔH = 63 J/g.

pTHF-bisBTA (***4c***). A solution of EDC (0.54 mmol, 105 mg) in 15 mL of dry $CHCl_3$ was added to an ice cooled stirred solution of **2c** (0.4 mmol, 173 mg), DMAP (0.54 mmol, 66 mg), and **3c** (0.18 mmol, 528 mg) in dry $CHCl_3$ (25 mL). The reaction mixture was allowed to warm to room temperature and stirred overnight. Then the mixture was diluted with $CHCl_3$ (50 mL) and washed successively with HCl (1 M, 50 mL), $NaHCO_3$ (10%, 20 mL), and $NaCl_{aq}$ (saturated, 20 mL). The product was concentrated and precipitated in cold ether and obtained as a white solid. Yield = 223 mg (64%). ^{1}H NMR ($CDCl_3$): δ 8.32 (ArH, s, 6H), 7.40 (NH, s, 2H), 6.81 (NH, s, 4H), 3.57 (CH_2NH, t, 8H), 3.41 (OCH_2CH_2, t, 83.17H) 3.24 ($NHCH_2(CH_2)_2O$, t, 4H), 2.56 (OCH_2CH_2, m, 83.21H)1.88 ($OCH_2CH_2CH_2NH$, m, 4H), 1.70−1.27 (alkyl, 42H), 0.87 (CH_3, t, 12H). ^{13}C NMR ($CDCl_3$): δ 165.8 135.4, 128.0, 70.6, 40.1, 31.6, 29.3, 26.4, 22.5, 14.0. IR: ν (cm^{-1}): 3241 (N−H stretch), 1640 (amide I), 1557 (amide II). GPC: M_n = 4135 g/mol, M_w = 7055 g/mol, PDI = 1.7. DSC (40 K/min): T = 122 °C, ΔH = 1.9 J/g.

5-Ethoxycyclooctene (***6***). Cyclooctadiene (10.0 g, 92.5 mmol) was dissolved in 250 mL of ethanol and added dropwise to a suspension of $Hg(OAc)_2$ (29.5 g, 92.5 mmol) in 250 mL of ethanol and stirred for 1 h at room temperature. Subsequently, 200 mL of NaOH (2M) was added to the solution followed by the dropwise addition of a solution of $NaBH_4$ (3.78 g, 100 mmol) in 200 mL of NaOH (2M) and stirred for 1 h at room temperature. Ethanol was removed *in vacuo* followed by the addition of NaCl (25 g). The aqueous solution was washed two times with 250 mL of diethyl ether. The organic layers were collected and washed two times with 300 mL of $NaCl_{aq}$ (saturated) and dried over $MgSO_4$. Diethyl ether was removed *in vacuo*, and the product was purified by column chromatography (silica gel 40−63 μm, 60 Å $CHCl_3$/MeOH, 95/5, R_f = 0.4). ^{1}H NMR (400 MHz, $CDCl_3$): δ 5.75−5.55 (m, 2H, $-CH{=}CH-$), 3.5−3.4 (m, 2H, $-O-CH_2CH_3$), 3.38−3.35 (m, 1H, $(CH_2)_2-CH-O-$), 2.39−1.3 (m, 10H, alkyl), 1.26−1.1 (m, 3H, $-O-CH_2CH_3$). ^{13}C NMR (100 MHz, $CDCl_3$): δ 130.8 (*C*=C), 129.5 (C=*C*), 80.3 ($(CH_2)CH$), 63.5 (OCH_2CH_3), 34.4, 33.6, 29.7, 26.3, 25.8, 24.0, 22.7, 15.6. GC/MS: calculated for $C_{10}H_{18}O$ (*m*/*z*) 154.25; found 154.

General Procedure for the Ring-Opening Metathesis Polymerization of Cyclic Olefins in the Presence of a Chain Transfer Agent. The reactions were carried out in "dry" and oxygen poor toluene (oxygen was reduced by purging with argon) under an argon atmosphere. The monomers, or mixtures of monomers, were dissolved together with the chain transfer agent in toluene. The reaction mixtures were stirred and heated to 55 °C. Subsequently, the Grubbs second-generation catalyst was added. After 18 h the reaction mixtures were cooled down to room temperature. The reaction mixtures were concentrated *in vacuo*, and the polymers were precipitated from toluene in cold methanol. White/yellowish powdery or waxy solids were obtained by filtration or decantation in a typical yield of about 90%. All polymers were synthesized using similar amounts and ratios of monomer, chain transfer agent, and catalyst at the same molar concentration.

p(CO) Bis-phthalimide (***8d***). Cyclooctene (1.41 g, 12.8 mmol) was dissolved together with *N*,*N*′-(1,20-eicos-10-endiyl)-bis-(isoindole-1,3-dione) (0.37 g, 0.641 mmol) in 5 mL of toluene. Subsequently, a solution of Grubbs' second-generation initiator (2.17 mg, 0.00256 mmol) was added. The reaction mixture was stirred for 18 h at 55 °C. The reaction mixture was concentrated and precipitated from toluene in methanol. The polymer was obtained by filtration as a white powder. Yield = 95%. ^{1}H NMR (400 MHz, $CDCl_3$): δ 7.82 (m, 4H, ArH), 7.72 (m, 4H, ArH), 5.39 (m, 2H, $CHCH_2$), 3.73 (t, 4H, $(CO)_2NCH_2$)), 1.97 (m, 4H, $CHCH_2$), 1.64−1.15 (alkyl). M_n = 2812 g/mol (^{1}H NMR).

p(CO-co-25%ECO) Bis-phthalimide (***8e***). Yield = 94%. ^{1}H NMR (400 MHz, $CDCl_3$): δ 7.89 (m, 4H, ArH), 7.81 (m, 4H, ArH), 5.40 (m, 2H, C*H*CH_2), 3.75 (t, 4H, $(CO)_2NCH_2$)) 3.50−3.40 (m, n2H, −O−C*H*$_2CH_3$), 3.38−3.35 (m, 1H, $(CH_2)_2$−C*H*−O−), 2.45−0.88 (alkyl). M_n = 2652 g/mol (^{1}H NMR).

p(CO-co-50%ECO) Bis-phthalimide (***8f***). Yield = 90%. ^{1}H NMR (400 MHz, $CDCl_3$): δ 7.87 (m, 4H, ArH), 7.75 (m, 4H, ArH), 5.40 (m, 2H, C*H*CH_2), 3.73 (t, 4H, $(CO)_2NCH_2$)) 3.50−3.40 (m, 2H, −O−C*H*$_2CH_3$), 3.38−3.35 (m, 1H, $(CH_2)_2$−C*H*−O−), 2.45−0.88 (alkyl). M_n = 2600 g/mol (^{1}H NMR).

p(ECO) Bis-phthalimide (***8g***). Yield = 85%. ^{1}H NMR (400 MHz, $CDCl_3$): δ 7.84 (m, 4H, ArH), 7.72 (m, 4H, ArH), 5.40 (m, 2H, C*H*CH_2), 3.65 (t, 4H, $(CO)_2NCH_2$)) 3.58−3.40 (m, 2H, −O−C*H*$_2CH_3$), 3.38−3.35 (m, 1H, $(CH_2)_2$−C*H*−O−), 2.45−0.88 (alkyl). M_n = 2348 g/mol (^{1}H NMR).

General Procedure for Synthesis of Amine End-Functionalized Polymers. The following procedure was used for all phthalimide end-capped polymers using the same reaction conditions.

p(CO) Bis-amine (***3d***). Hydrazine monohydrate and p(CO) bis-phthalimide (**8d**) (1.3 g, 0.46 mmol) were dissolved in 20 mL of THF and heated at 90 °C for 18 h. The reaction mixture was allowed to cool down to room temperature. THF and the excess of hydrazine were removed *in vacuo*. Then 50 mL of chloroform was added to the mixture. The mixture was washed three times with 75 mL of NaOH (1 M) and two times with 75 mL of $NaCl_{aq}$(sat.). The organic layer was dried over $MgSO_4$ and the solvent was removed *in vacuo*. Yield = 95%. ^{1}H NMR (400 MHz, $CDCl_3$): δ 5.39 (m, 2H, C*H*CH_2), 2.65 (t, 2H, −C*H*$_2NH_2$) 1.97 (m, 4H, CHC*H*$_2$), 1.64−1.15 (alkyl). M_n = 2518 g/mol (^{1}H NMR).

p(CO-co-25%ECO) Bis-amine (***3e***). Yield = 93%. ^{1}H NMR (400 MHz, $CDCl_3$): δ 5.40 (m, 2H, C*H*CH_2), 3.5−3.4 (m, 2H, −O−C*H*$_2CH_3$), 3.38−3.35 (m, 1H, $(CH_2)_2$−C*H*−O−), 2.65 (t, 2H, −C*H*$_2NH_2$), 2.40−0.88 (alkyl). M_n = 2358 g/mol (^{1}H NMR).

p(CO-co-50%ECO) Bis-amine (***3f***). Yield = 90%. ^{1}H NMR (400 MHz, $CDCl_3$): δ 5.40 (m, 2H, C*H*CH_2), 3.5−3.4 (m, 2H, −O−C*H*$_2CH_3$), 3.38−3.35 (m, 1H, $(CH_2)_2$−C*H*−O−), 2.62 (t, 2H, −C*H*$_2NH_2$), 2.40−0.88 (alkyl). M_n = 2308 g/mol (^{1}H NMR).

p(ECO) Bis-amine (***3g***). Yield = 80%. ^{1}H NMR (400 MHz, $CDCl_3$): δ 5.40 (m, 2H, C*H*CH_2), 3.5−3.4 (m, 2H, −O−C*H*$_2CH_3$), 3.38−3.35 (m, 1H, $(CH_2)_2$−C*H*−O−), 2.60 (t, 2H, −C*H*$_2NH_2$), 2.39−0.88 (alkyl). M_n = 2056 g/mol (^{1}H NMR).

General Procedure for Benzene-1,3,5-tricarboxamide End-Capped Polymers. The following procedure was used for polymers **4d**−**4f** using the same reaction conditions.

p(CO)-bis-BTA (***4d***). Polymer **3d** (0.75 g, 0.35 mmol), 3,5-bis(3*S*)-(3,7-dimethyloctylaminocarbonyl)benzoic acid (0.28 g, 0.78 mmol), *N*,*N*′-dicyclohexylcarbodiimide (DCC) (0.23 g, 1.5 mmol), and 4-(dimethylamino)pyridine *p*-toluenesulfonate (DPTS) (0.169 g, 1.5 mmol) were dissolved in 25 mL of $CHCl_3$ and stirred for 18 h at room temperature. The reaction mixture was concentrated to 3 mL and precipitated in methanol twice. Yield = 85%. ^{1}H NMR ($CDCl_3$): δ 8.34 (s, 6H, ArH), 6.43 (t, 6H, NH), 5.38−5.30 (m, 2H, C*H*CH_2), 3.47 (m, 12H, CONHC*H*$_2$), 1.97 (m, 4H, CHC*H*$_2$), 1.64−1.15 (alkyl), 0.88 (t, 12H, CH_3). ^{13}C NMR ($CDCl_3$): δ 165.8 (C═O), 135.5 (ArC), 130.3 (ArC), 129.8 (C═C), 128.0 (C═C), 40.5 (NH−CH_2), 32.6, 31.8, 29.6, 28.9, 27.1, 22.4, 14.0. IR: ν (cm^{-1}) 3241 (N−H stretch), 1640 (amide I), 1560 (amide II). GPC: M_n = 5.5 kg/mol, M_w = 6.9 kg/mol, PDI = 1.25.

p(CO-co-25%ECO)-bisBTA (***4e***). Yield = 75%. ^{1}H NMR ($CDCl_3$): δ 8.4 (s, 6H, ArH), 6.53 (t, 6H, NH), 5.38−5.30 (m, 2H, C*H*CH_2), 3.5−3.4 (m, 2H, −O−C*H*$_2CH_3$), 3.47 (m, 12H, CONHC*H*$_2$), 3.38−3.35 (m, 1H, $(CH_2)_2$−C*H*−O−), 1.97 (m, 4H, CHC*H*$_2$), 1.64−1.15 (alkyl), 0.88 (t, 12H, CH_3). ^{13}C NMR ($CDCl_3$): δ 165.8 (C═O), 135.4 (ArC), 130.7 (ArC), 129.7 (C═C), 127.9 (C═C), 64.1 (*C*H−O−*C*H_2CH_3), 39.2 (NH−CH_2), 38.5, 36.6, 34.1, 30.7, 32.7, 29.5, 28.6, 28.0, 27.2, 25.4, 22.7, 19.9, 14.8. IR: ν (cm^{-1}) 3245 (N−H stretch), 1641 (amide I), 1559 (amide II). GPC: M_n = 6.5 kg/mol, M_w = 10.2 kg/mol, PDI = 1.55.

p(CO-co-50%ECO)-bisBTA (***4f***). Yield = 70%. ^{1}H NMR ($CDCl_3$): δ 8.36 (s, 6H, ArH), 6.65 (t, 6H, NH), 5.38−5.30 (m, 2H, C*H*CH_2), 3.5−3.4 (m, 2H, −O−C*H*$_2CH_3$), 3.47 (m, 12H, CONHC*H*$_2$), 3.38−3.35 (m, 1H, $(CH_2)_2$−C*H*-O−), 1.97 (m, 4H, CHC*H*$_2$), 1.64−1.15 (alkyl), 0.88 (t, 12H, CH_3). ^{13}C NMR ($CDCl_3$): δ 165.6 (C═O), 135.3 (ArC), 130.3 (ArC), 129.7 (C═C), 127.9 (C═C), 64.1 (*C*H−O−*C*H_2CH_3), 40.4 (NH−CH_2), 38.5, 36.2, 34.1, 30.7, 29.5, 28.6, 27.9, 27.2, 25.4, 22.8, 19.9, 14.8. IR: ν (cm^{-1}) 3245 (N−H stretch), 1641 (amide I), 1559 (amide II). GPC: M_n = 8.0 kg/mol, M_w = 15.0 kg/mol, PDI = 1.87.

p(ECO)-bisBTA (***4g***). A solution of EDC (0.62 mmol, 119 mg) in 15 mL of dry $CHCl_3$ was added to an ice cooled stirred solution of compound **20** (0.62 mmol, 271 mg), DMAP (0.62 mmol, 76 mg), and polymer **3g** (0.28 mmol, 1 g) in dry $CHCl_3$ (25 mL). The reaction mixture was allowed to warm to room temperature and stirred overnight. Then the mixture was diluted with $CHCl_3$ (50 mL) and washed successively with HCl (1 M, 50 mL), $NaHCO_3$ (10%, 20 mL), and $NaCl_{aq}$ (saturated, 20 mL). $CHCl_3$ was removed *in vacuo*. The product dissolved in 2 mL of chloroform and subsequently precipitated in cold ether and obtained as a white/yellowish solid. Yield = 80%. ^{1}H NMR ($CDCl_3$): δ 8.42 (s, 6H, ArH), 6.7 (t, 6H, NH), 5.38−5.30 (m, 2H, C*H*CH_2), 3.5−3.4 (m, 2H, −O−C*H*$_2CH_3$), 3.47 (m, 12H, CONHC*H*$_2$), 3.38−3.34 (m, 1H, $(CH_2)_2$−C*H*−O−), 1.97 (m, 4H, CHC*H*$_2$), 1.64−1.15 (alkyl), 0.88 (t, 12H, CH_3). ^{13}C NMR ($CDCl_3$): δ 165.6 (C═O), 135.3 (ArC), 130.3 (ArC), 129.7 (C═C), 127.9 (C═C), 64.1 (*C*H−O−*C*H_2CH_3), 40.4 (NH−CH_2), 38.5, 36.2, 34.1, 30.7, 29.5, 28.6, 27.9, 27.2, 25.4, 22.8, 19.9, 14.8. IR: ν (cm^{-1}) 3243 (N−H stretch), 1641 (amide I), 1558 (amide II). GPC: M_n = 6.7 kg/mol, M_w = 8.9 kg/mol, PDI = 1.32.

Results and Discussion

Polarity Effects in Dilute Solutions of (*R*)-1. We previously studied in detail the self-assembly of BTA (*R*)-**1** in dilute solutions.[48] In heptane, the formation of helical columnar aggregates is characterized by a λ_{max} of 192 nm in UV and a strong Cotton effect at 223 nm with $\Delta\varepsilon$ = +43 L/(mol cm).[48,54] In acetonitrile, a red shift in UV to 208 nm with a corresponding disappearance of the Cotton effect was attributed to the loss of intermolecular hydrogen bonds. Moreover, temperature-dependent CD measurements showed that the temperature-dependent aggregation could be described by a nucleation−elongation mechanism.[48,55] In a nucleation−elongation mechanism, polymerization can only occur after nucleation (activation) of the monomer. This relatively unfavorable nucleation step precedes the elongation regime of the polymerization and is governed by a dimensionless activation constant, K_a. A smaller K_a value corresponds to a higher degree of cooperativity. The addition of the monomer to the growing chain in the elongation regime is governed by an equilibrium constant K_e, which can be expressed as a function of an elongation enthalpy, h_e, and an elongation temperature, T_e. This T_e separates the two polymerization regimes (i.e., the nucleation and elongation regime), while the elongation enthalpy is the enthalpy that is released due to the formation of noncovalent intermolecular interactions during the elongation phase. Quantitative data on the self-assembly process were obtained by fitting the temperature-dependent CD data to a nucleation−elongation model developed by van der Schoot.[48,55]

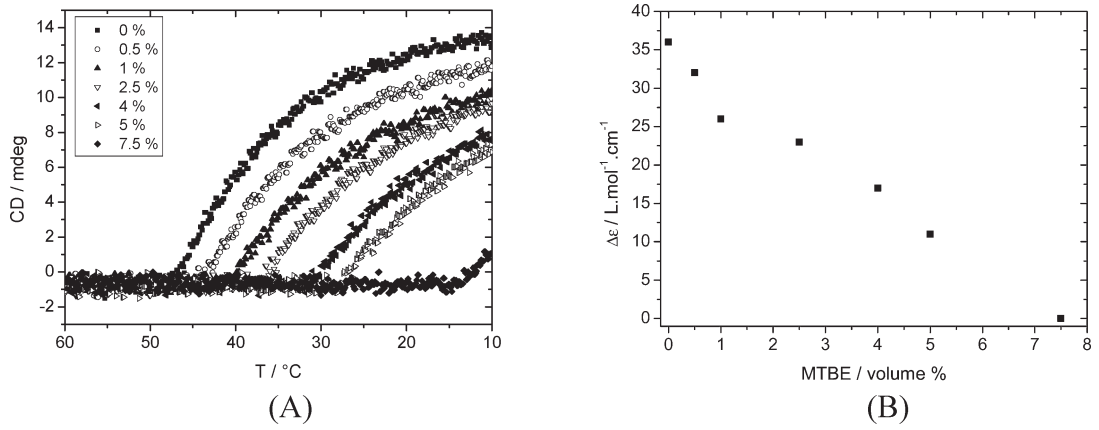

Figure 2. (A) CD cooling curves of (*R*)-**1** in MTBE/MCH mixtures at $c = 10\,\mu$M. (B) Decrease of $\Delta\varepsilon$ as a function of the amount of MTBE added (at 20 °C).

Table 1. Thermodynamic Parameters for the Self-Assembly of (*R*)-1 in Mixtures of MTBE/MCH ($c = 10\,\mu$M)

MTBE in MCH [vol %]	h_e [kJ/mol]	T_e [°C]
0	−64.4	48
0.5	−58.8	45
1	−53.3	41
2.5	−47.5	36
4	−46.7	33
5	−36.6	28
7.5	−28.0	10

We selected methyl *tert*-butyl ether (MTBE) as a solvent capable of interfering with the intermolecular hydrogen bonds because of its low UV cutoff and boiling point of 55 °C. According to UV, (*R*)-**1** is molecularly dissolved in MTBE ($c = 10\,\mu$M) at room temperature as evidenced by λ_{max} at 208 nm (Figure S1). Moreover, no Cotton effect is observed in MTBE (Figure S2). We anticipated that the addition of small amounts of MTBE to methylcyclohexane (MCH), in which (*R*)-**1** forms long stable aggregates, reduces the average aggregate size and increases the fraction of (*R*)-**1** in the monomeric form.[54] CD spectroscopy on (*R*)-**1** in mixtures of MCH and MTBE was performed while the amount of MTBE was increased from 0% to 7.5% v/v. The concentration was kept constant at 10 μM. At room temperature, a linear decrease of the CD effect at 223 nm is observed with increasing the amount of MTBE (Figure 2B). After the addition of 7.5% v/v MTBE, the CD effect is completely lost which indicates that this solvent mixture is unable to stabilize the 3-fold hydrogen bonds required for the helical aggregate formation.

We then performed temperature-dependent CD spectroscopy measurements of (*R*)-**1** in mixtures of MCH and MTBE. Probing the CD effect at 223 nm shows the sudden appearance of a CD effect upon cooling the solutions from 60 °C, at which temperatures (*R*)-**1** is molecularly dissolved, to 10 °C (cooling rate = 5 °C/min) as is visible in Figure 2A. Nonsigmoidal curves are found for all mixtures, indicating a nucleation−elongation type self-assembly process, even when significant amounts of MTBE are added. The elongation temperature, T_e, is lowered, and the slope of the curve (at the T_e), which is proportional to h_e, is decreased upon increasing MTBE amounts.

Fitting the CD cooling curves to the nucleation−elongation model allows to derive T_e and h_e values as a function of the amount of MTBE added (see Supporting Information for details on the procedure and Figure S3). The data are summarized in Table 1. As expected, both T_e and h_e decrease. In fact, h_e is reduced to less than half of its original value when 7.5% of MTBE is added, meaning that less enthalpy is released when aggregates are formed in more polar media. This reduced enthalpy release means that weaker hydrogen bonds are formed upon elongation. The reduction of the T_e is a result of the solvent composition, which possesses better solvability properties upon the addition of MTBE. Therefore, a lower temperature is needed to form and stabilize aggregates.

Synthesis and Characterization of BTA End-Capped Polymers of Different Polarity. From our solution studies, we observed that a more polar environment causes a decrease in the stability of aggregates, resulting in smaller values for the degree of aggregation, h_e, and a lower T_e. As this may have dramatic effects on the properties of functional polymers end-capped with a BTA unit, we systematically varied the polymer backbone polarity to study its effect on BTA aggregate formation in the solid state. We first selected readily accessible polymers such as apolar pEB, medium polar pTHF, and polar pCL, all commercially available as hydroxy telechelic polymers. Both pEB—an amorphous apolar polymer- and pTHF—a semicrystalline polyether-, were chosen because of their promising ability to behave as the soft part in supramolecular thermoplastic elastomers.[29,33,56] PCL is a particularly interesting backbone because of its biocompatible and biodegradable character.[57] Amine telechelics **3a**−**c** were readily accessible via standard synthetic procedures and were subsequently coupled to BTA precursors (**2a**,**b**) using EDC as the coupling agent in the presence of DMAP (Scheme 2).

Polymers **4a**−**c** were obtained in an average yield of 60% and isolated in high purity as evidenced by ^{1}H NMR and ^{13}C NMR. As an example, the ^{1}H NMR spectrum of pEB-bisBTA (**4a**) is depicted in Figure 3. The signature signals of the amide−N*H* and the Ar−*H* of the BTA part are found at $\delta = 6.4$ and 8.4 ppm, respectively. GPC traces (polystyrene calibrated) showed molecular weights of 6.2, 12.4, and 4.2 kDa for **4a**, **4b**, and **4c**, respectively, and low polydispersity indexes for all three polymers (Table 2).

In order to systematically tune the backbone, we also designed amine telechelic polymers **3d**−**g** (Scheme 1) where the polarity can be tuned by mixing two monomers namely cyclooctene (CO) and the more polar 5-ethoxycyclooctene (ECO, **6**). The latter is accessible in a one-step synthesis starting from 1,5-cyclooctadiene. The ether group in ECO not only increases the polarity but also acts as a hydrogen bond acceptor that might destabilize BTA aggregates, similarly to the effect of MTBE in the aggregation of (*R*)-**1**

(vide supra). The monomers CO and ECO were selected because of their well-known reactivity in ROMP.[58] Moreover, similar ring strains were expected, which will result in the formation of random copolymers (Scheme 3). The BTA end-groups were introduced by using a phthalimide-based bifunctional chain transfer reagent (CTA) (Scheme 3). Conceptually, ROMP of a cyclic olefin in the presence of a symmetric CTA agent with two functional groups can be viewed as growing a polymer in between these groups. The phthalimide-based CTA (**7**) was used for two reasons: (i) the phthalimide groups do not interfere with the ruthenium catalyst during polymerization, in contrast to BTA functionalized CTAs,[59] and (ii) phthalimide groups give easy access to amine end-groups (Scheme 3).

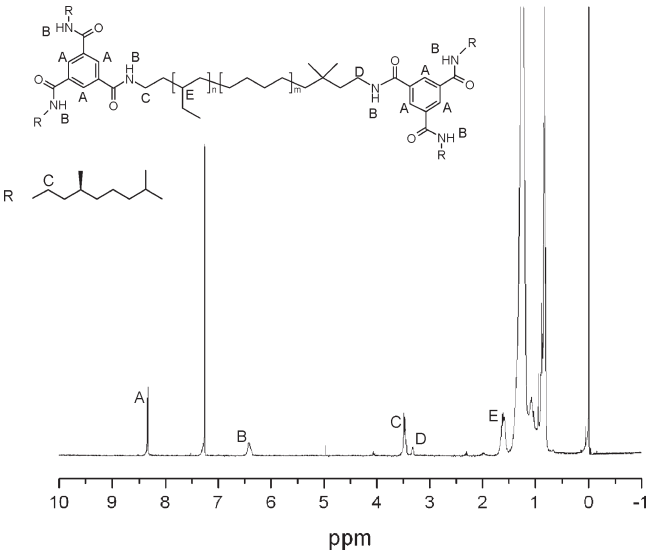

Figure 3. ^{1}H NMR spectrum of pEB-bisBTA (**4b**) in $CDCl_3$.

Four different phthalimide end-capped polymers were synthesized using CO and ECO as monomers, namely p(CO) **8d**, p(CO-*co*-25%ECO) **8e**, p(CO-*co*-50%ECO) **8f**, and p-(ECO) **8g** (Scheme 3). All polymerizations were performed in dry toluene for 18 h at 55 °C under an argon atmosphere. A monomer:initiator ratio of 5000:1 was used with concentrations of about 2 M, allowing the end-group functionality to be >99%.[49,60] According to ^{1}H NMR, the observed ratio of CO:ECO in polymers **4e**,**f** is identical to the feed ratio, suggesting that the reactivity of both monomers is indeed equal (Table 2). Subsequently, the phthalimide groups were reduced to amines in a solution of hydrazine monohydrate in THF at reflux temperature. Telechelics **3d**−**g** were then coupled to the chiral BTA precursor **2c** to form BTA end-capped polymers **4d**−**g**. Polymers **4d**−**4f** were synthesized using DCC as peptide coupling agent and DPTS as the catalyst. Polymers **4d**−**4f** were purified by precipitation in methanol twice. Polymer **4g** was synthesized using EDC as the coupling agent in the presence of DMAP for a more convenient work-up. Polymers **4d**−**g** were obtained in high yield and characterized with ^{1}H NMR, ^{13}C NMR, and GPC. The results are summarized in Table 2.

According to ^{1}H NMR and SEC all polymers had a similar molecular weight of around 4 kg/mol with relatively low polydispersity of 1.4 (Table 2). The molecular weight of polymers **4a**−**g** is also easily estimated with ^{1}H NMR by comparing signals from the aromatic BTA motif and various signals from the repeating unit. The degree of polymerization is around 20, which resulted in similar molecular weights

Table 2. ^{1}H NMR, GPC, and DSC Data of Polymers 4a−g

		obsd ratio											
polymer	backbone	*n* [%]	*m* [%]	yield [%]	M_n[a] [kg/mol]	M_n[b] [kg/mol]	M_w[b] [kg/mol]	PDI	T_g [°C]	T_{m1} [°C]	ΔH [J/g]	T_{m2} [°C]	ΔH [J/g]
4a	pEB	n.a.[c]	n.a.	60	4.4	6.2	6.9	1.12	−60			210	2.63
4b	pCL	n.a	n.a.	60	5.8	12.4	14.2	1.15		44	58		
4c	pTHF	n.a.	n.a.	50	3.9	4.1	7.1	1.7				122	1.89
4d	pCO	100	0	85	3.8	5.5	6.9	1.25	−80	45	24	190	3.3
4e	p(CO-*co*-25%ECO)	75	25	75	3.6	6.5	10.2	1.55	−70	25	8	165	0.9
4f	p(CO-*co*-50%ECO)	50	50	70	3.6	8.0	15.0	1.87				150	0.6
4g	pECO	0	100	80	3.3	6.7	8.9	1.32				130	0.34

[a] Determined by ^{1}H NMR. [b] Determined by GPC. [c] n.a. = not applicable.

Scheme 2. Synthesis of pEB-bisBTA (4a), pTHF-bisBTA (4b), and pCL-bisBTA (4c)

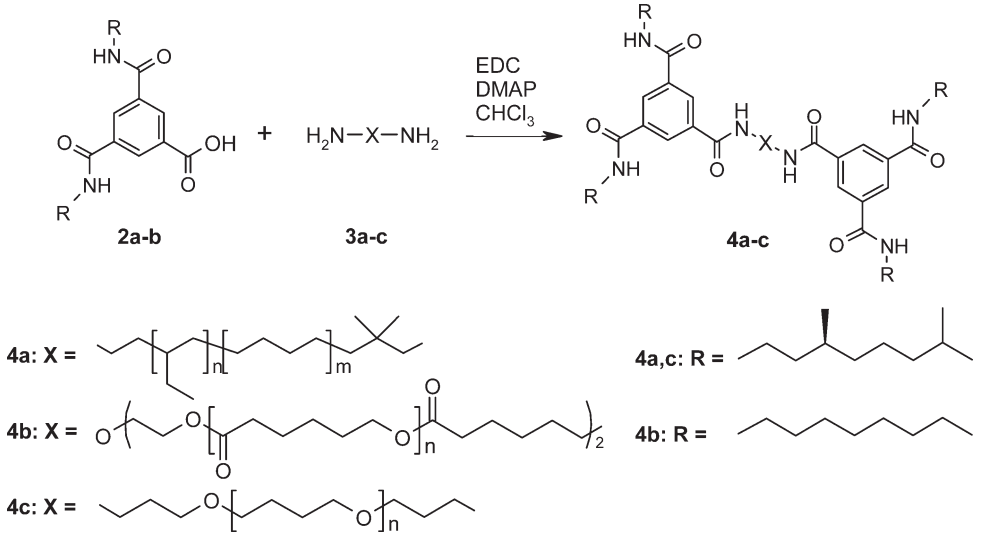

Scheme 3. Synthetic Approach to Polymers 4d−g with Tunable Polymer's Backbone Polarity

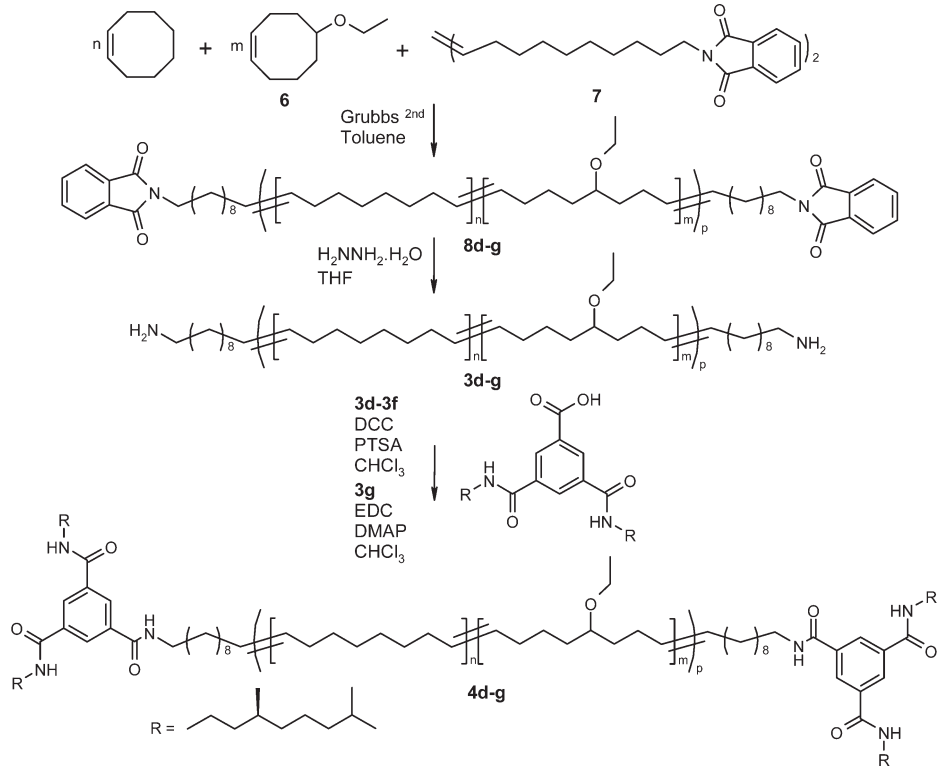

compared to the functionalized commercially available telechelics (**4a**−**c**). Therefore, we can easily assess the influence of backbone polarity on the properties of BTA end-capped polymers and exclude effects of molecular weight.

Thermal Properties of BTA-Functionalized Telechelics (4a−**g).** We previously observed that pEB, a viscous liquid at room temperature, becomes a solid after functionalization with a BTA unit with material properties similar to that of a soft rubber.[38] In contrast, pCL and pTHF do not show any remarkable changes in material properties after functionalization with the BTA unit. BTA-functionalized telechelics **4d**, **e** did also not show any significant change in their physical appearance compared to **3d**,**e**. In contrast, amorphous polymers **4f**,**g** did change after functionalization from sticky viscous fluids to elastic solids. This change in physical appearance is indicative for the presence of phase-segregated nanorods that act as physical cross-linkers.

To rationalize the differences between the different polymers, we performed DSC and polarization optical microscopy (POM) measurements on samples of BTA end-capped polymers **4a**−**g.** The DSC data for polymers **4a**−**g** were derived from the third heating run (40 K/min), and the results are summarized in Table 2. We selected the third heating run as the isotropic phase transitions were most clearly visible at the high rate of 40 K/min (see Figure S4). The DSC trace of pEB-bisBTA (**4a**) showed a T_g at −60 °C and a small transition around 195−215 °C (ΔH = 2.63 J/g) (see Table 2). With POM, we observed a mobile, birefringent texture typical for a nematic phase starting from 60 °C up to the clearing temperature around 200 °C, allowing us to attribute the transition at 195−215 °C to a transition into the isotropic state. In contrast, the DSC trace of pCL-bisBTA (**4b**) showed only one phase transition at 44 °C (ΔH = 58 J/g). This transition is related to the melting of the pCL backbone. The DSC trace of pTHF-bisBTA (**4c**) showed a small transition around 115−125 °C. Remarkably, no phase transition is observed that can be attributed to the melting of the pTHF backbone, typically found at 23 °C (for pTHF diol, M_n = 3000 g/mol).[61] This indicates that the presence of the BTA unit hinders the crystallization of the pTHF backbone. With POM, we observed a mobile, birefringent texture indicative for a nematic phase starting from around 50 °C up to the clearing temperature around 120 °C.

In terms of backbone polarity, pEB-bisBTA (**4a**) and pCO-bisBTA (**4d**) are very similar, i.e., nonpolar, although pCO is a semicrystalline polymer (T_m = 50 °C, T_g = −90 °C) while pEB is amorphous. If the formation of BTA aggregates in the solid state is primarily governed by polarity effects, similar thermal properties could be expected for **4a** and **4d**. Indeed, the DSC trace of **4d** showed a T_g at −80 °C, a phase transition around 45 °C (ΔH = 24 J/g) corresponding to the melting of the pCO polymer and a small transition around 190 °C (ΔH = 3.3 J/g) (Table 2). With POM, we observed a mobile, birefringent texture typical for a nematic phase starting from 80 °C up to the clearing temperature around 190 °C. Clearly, the mobile birefringent phase and an isotropic transition around 190−210 °C for **4a**,**d** show the similarities of these polymer's thermal behavior. Moreover, pECO-bisBTA (**4g**) resembles pTHF-bisBTA (**4c**) with regard to its backbone polarity, and also in this case the thermal behavior is rather similar. The DSC trace of compound **4g** showed a small phase transition at 130 °C (ΔH = 0.34 J/g), and POM revealed a mobile birefringent texture starting from around room temperature up to its clearing temperature of 130 °C, which is close to the clearing temperature of 120 °C found for pTHF-bisBTA (**4c**).

As expected, copolymers p(CO-*co*-25%ECO)-bisBTA (**4e**) and p(CO-*co*-50%ECO)-bisBTA (**4f**) show a thermal behavior that is intermediate to that of **4d** and **4g**. P(CO-*co*-25%ECO)-bisBTA showed a T_g at −70 °C, a phase transition around 25 °C (ΔH = 8 J/g) and a small transition around 165 °C (ΔH = 0.9 J/g). POM showed a mobile birefringent texture starting from 50 °C up to clearing temperature of 165 °C. The DSC trace of compound **4f**

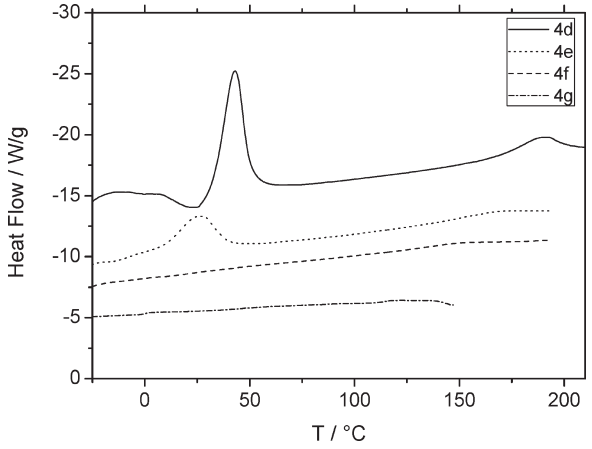

Figure 4. DSC traces of polymers **4d**−**g**.

showed a small phase transition at 150 °C (ΔH = 0.6 J/g), and POM revealed a mobile birefringent texture starting from around room temperature up to its clearing temperature at 150 °C. In fact, an interesting trend in the thermal behavior of **4d**−**4g** can be distinguished: polymers containing more ECO monomer are less crystalline, and the liquid crystalline to isotropic phase transition temperature decreases. The former is related to the presence of ECO monomers that prevent the crystallization—p(ECO) is an amorphous viscous liquid—while the latter appears to be connected to the increase in the backbone's polarity and concomitant destabilization of the BTA aggregates.

CD Spectroscopy in the Solid State. Since BTAs form helical stacks with preferred helicity in dilute solution, we wondered if the propensity to form helical stacks is retained when BTAs are embedded in a polymer matrix. We studied chiral polymers **4a**,**c**−**g** with CD spectroscopy to verify the presence of columnar helical structures as found for (*R*)-**1** in dilute solution. Functionalized pCL (**4b**) was not functionalized with chiral side chains because the BTA motif is unable to form helical structures when embedded in a pCL matrix.[62] Films of **4a**,**c**−**g** with a thickness of 250−650 nm were spin-coated from a $CHCl_3$ solution on quartz plates. CD spectra were recorded at room temperature and are shown in Figure 4. A clear Cotton effect was observed for **4a**,**c**−**g**, similar in shape and opposite in sign as observed for **1**. The latter was expected since an *R*-configuration was used for **1** while the polymers were functionalized with BTA precursors comprising the *S*-configuration. Moreover, the chirality of the BTA (*S*) determines the helicity in the stacks as seen with BTAs in solution.[54] The CD effect was independent of the orientation of the quartz plate with respect with the beam, excluding linear dichroism effects. This suggests that the helical order present in a dilute solution of **1** is also present in the solid-state of **4a**,**c**−**g**. The CD effect of pCO-bisBTA (**4d**) is about twice as large compared to that of p(CO-*co*-50% ECO)-bisBTA (**4f**) and pECO-bisBTA (**4g**) (Figure 5). This suggests that the BTA motifs in polar polymers **4f**,**g** are relatively more present in the monomeric form instead of in the aggregated form, leading to the formation of smaller or fewer stacks.

DSC and POM results of polymers **4a**,**c**−**g** showed a decrease of the solid to isotropic phase transitions with increasing polarity. Temperature-dependent CD measurements on polymers **4a**,**c**−**g** can elucidate if this difference in thermal behavior is related to the helical aggregation of BTAs embedded in the polymer matrix. We selected pTHF-bisBTA (**4c**) and pCO-bisBTA (**4d**) because of their

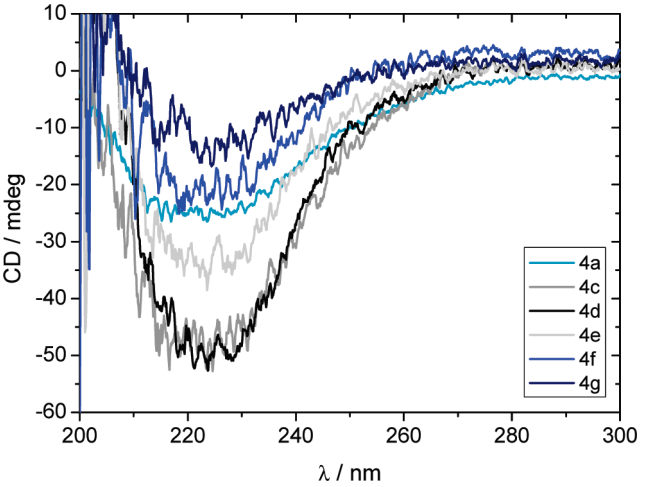

Figure 5. CD spectra of spin-coated films of **4a**,**c**−**g**. Film thickness of **4a**,**c**−**g** is 320, 650, 600, 550, 500, and 260 nm, respectively (at room temperature).

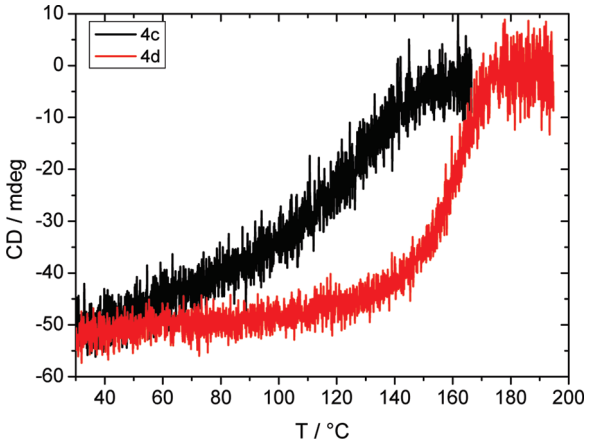

Figure 6. CD intensity at λ = 225 nm versus temperature of spin-coated films of **4c**,**d**.

large difference in polarity and their similar film thicknesses. The temperature was increased from 30 to 200 °C with a rate of 5 °C/min. The CD effect was monitored upon heating at λ_{max} = 225 nm and plotted versus temperature (Figure 6).

Both polymers show a decrease of the CD effect upon heating. The CD effect of pTHF-bisBTA (**4c**) decreases gradually and is completely absent above 140 °C. Apolar polymer pCO-bisBTA (**4d**) shows a more sudden decrease of the CD effect and the decrease starts at a higher temperature and disappears at around 180 °C. The CD effects of pTHF-bisBTA and pCO-bisBTA disappear at similar temperatures at which the mesophase to isotropic transition was observed in DSC and POM (120 and 190 °C, respectively). This indicates that indeed this phase transition is related to the disappearance of the helical arrangement of BTAs in the polymer matrix. We also observe a difference in the slope of the CD effect upon heating. The slope of **4d** is steeper compared to the slope of the more polar polymer **4c**. A similar difference in the slope is observed in cooling experiments of the monomeric BTA (**1**) dissolved in mixtures of MCH and MTBE (*vide supra*). With increasing concentration of MTBE and thus polarity, the slope of the CD effect upon cooling becomes less steep. The slope is related to the enthalpy change upon aggregation (h_e), which reflects the amount of energy that is released during the formation of hydrogen bonds. Assuming that the disassembly of BTAs in

4c,**d** upon heating (5 °C/min) occurs under thermodynamic conditions, we can conclude from the difference in the slope that hydrogen bonds are less strong in the more polar pTHF-bisBTA compared to hydrogen bonds in the apolar pCO-bisBTA.

IR Spectroscopy of BTA-Functionalized Polymers. The mesophase to isotropic transition observed in compounds **4a**,**c**−**g** appears to be connected to the loss of the intermolecular hydrogen bonds and corresponding disappearance of the BTA aggregates in the solid state, while for compound p(CL)-bisBTA (**4b**) no such transition was observed at all. To investigate this in more detail, we performed IR measurements on polymers **4a**−**g**, since this is a sensitive technique to investigate hydrogen bonding in the solid state.[47,51]

At room temperature, the solid-state IR spectrum of **4a** shows vibrations at positions typical for amides involved in 3-fold helical hydrogen bonds (ν(N−H) 3240 cm^{-1}, ν(amide I) 1642 cm^{-1}, and ν(amide II) 1562 cm^{-1}).[47,51] Variable temperature IR reveals shifting of the characteristic vibrations starting at 100 °C up to 200 °C (see Figure 7A,B). This allows us to attribute the phase transition around 200 °C to the loss of the 3-fold helical hydrogen bonds. In contrast, the vibrations typical for amides involved in 3-fold hydrogen-bonded arrangement were absent in case of pCL-bisBTA (**4b**) at room temperature. In fact, polymer **4b** showed a very broad N−H stretching vibration signal with a maximum peak height at 3330 cm^{-1} (Figure S5). Also, the distance between the amide I and amide II vibrations signals is relatively high, 1645−1535 cm^{-1}. Moreover, the amide I vibration signal is split up. The most likely reason is that the broad structure of the vibrational mode is caused by the superposition of many sharper bands of a variety of species, indicative for the presence of randomly ordered BTAs.[63] The IR spectrum of pTHF-bisBTA (**4c**) in the solid state at room temperature does again show vibrations at positions typical for amides involved in the 3-fold hydrogen-bonded arrangement. Variable temperature IR showed a gradual shifting of the characteristic vibrations starting at 95−120 °C and allowed us again to attribute the phase transition around 120 °C to the loss of 3-fold helical hydrogen bonds (see Figure 7A,B). At room temperature, polymers **4d**−**g** show also vibrations around the typical positions for amides involved in 3-fold hydrogen bonding. Variable temperature IR revealed a gradual shifting of the characteristic vibrations starting from room temperature up to the clearing temperature and allowed us to attribute the transitions (T_{m2}) observed in DSC to the loss of 3-fold helical hydrogen bonds. The position of the NH stretch and amide I vibration versus temperature is plotted in Figure 7A,B. A shift in wavenumber with increasing temperature, which becomes more intense at the clearing temperature, is observed for all four polymers. Compound **4d** has the most abrupt shift very close to the clearing temperature around 190 °C. In contrast, **4g** has a more gradual shift toward the clearing temperature at 130 °C. The characteristic vibrations for amides involved in 3-fold hydrogen bonding disappear with increasing temperature. Moreover, this occurs at a lower temperature for polymers consisting of more polar ethoxy side groups.

A significant difference is observed in the role of BTAs as physical cross-linker when coupled to pCL or the other polymers and copolymers. PEB-bisBTA (**4a**) has a clearing temperature close to the clearing temperature of (*R*)-**1** (236 °C).[54] This suggests that the aggregation of BTAs in **4a** is barely influenced by the presence of the polymer and therefore has the ability to form phase-segregated nanorods. This phase transition is observed at a much lower temperature for pTHF-bisBTA and is totally absent in pCL-bisBTA. The pCL polymer backbone of **4b** consists of many ester bonds and particularly the carbonyls are strong hydrogen-bonding accepting groups. The carbonyls compete with intermolecular hydrogen bonding, which results in weaker or no intermolecular hydrogen bonding of BTAs. Polymers **4d**−**g** showed a similar trend in which it was clearly shown that with increasing ether group content the stability of BTA aggregates decreases. This resulted in lower clearing temperatures that were a result of the loss of intramolecular hydrogen bonding and the loss of the helical arrangement, as evidenced by IR and CD spectroscopy.

Table 3. IR Spectroscopy Data of Compounds 1 and 4a−g Determined at 20 °C in the Solid State

compound	ν(N−H) [cm^{-1}]	ν(amide I) [cm^{-1}]	ν(amide II) [cm^{-1}]
1	3240	1642	1562
4a	3236	1637	1563
4b	3330	1645	1535
4c	3240	1642	1562
4d	3241	1640	1560
4e	3245	1641	1559
4f	3245	1641	1559
4g	3243	1641	1558

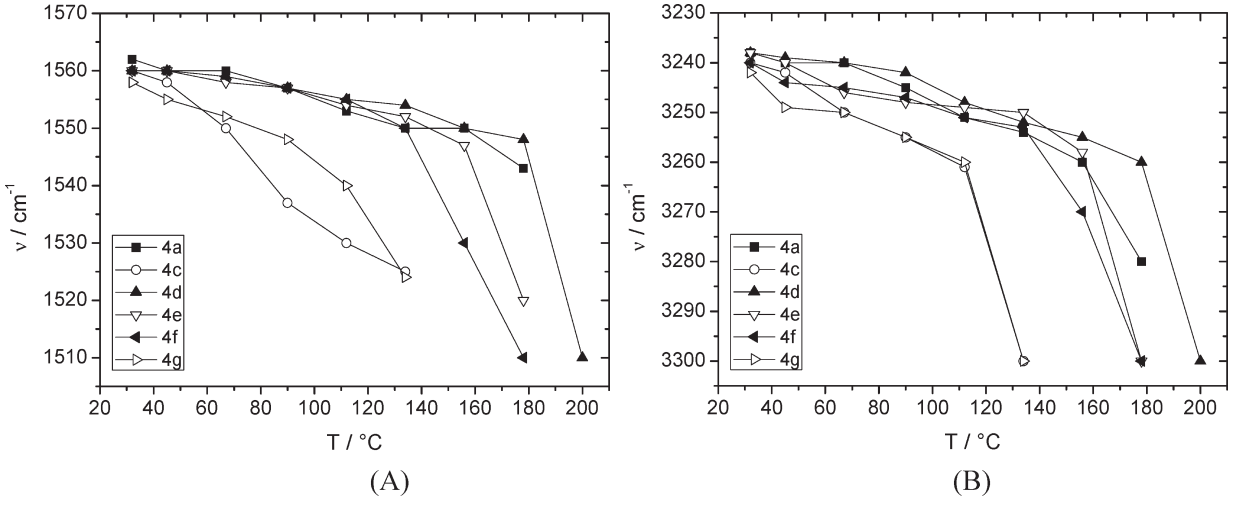

Figure 7. Infrared spectroscopy of **4a**,**c**−**g**. (A) Position of the amide I vibration versus temperature. (B) Position of the NH stretch vibration versus temperature.

Conclusions

In this systematic study, we show the influence of polarity on the hydrogen-bonded directed self-assembly of BTAs in dilute solution and on their ability to act as physical cross-linkers in polymeric systems. Apolar solvents like heptane or MCH stabilize intermolecular hydrogen bonding of BTAs, which result in the formation of stable helical aggregates even in very dilute conditions. Addition of small amounts of polar MTBE to solutions of BTAs in MCH resulted in a less stable system. This increase of polarity stimulates the presence of BTAs in the monomeric form, which results in a decrease of CD effect. The elongation temperature (T_e) decreases with increasing polarity because more polar solvent mixtures are more capable of stabilizing the monomers. Also, the enthalpy gain upon elongation decreases with increasing polarity indicating that less or weaker hydrogen bonds are formed in BTA aggregates. BTAs were already molecularly dissolved after the addition of 7.5 vol % MTBE in MCH at 20 °C.

The polarity of the solvent evidently plays an important role in the stabilization of BTA aggregates in dilute solutions. Since aggregation in dilute solutions is an indication for the formation of phase segregated nanorods in the solid state, we translated the effect of polarity in dilute solution to the solid state. Functionalization of the highly apolar pEB with BTAs resulted in a phase-segregated polymer. Unfortunately, functionalizing pCL with BTA motifs did not lead to any significant changes. DSC and IR confirmed the absence of BTA phase-segregated nanorods in pCL. Since pCL is a highly polar polymer, we assume that the oxygen atoms in the ester groups compete with intramolecular hydrogen bonding and therefore destabilize BTA aggregates. Anticipating on this hypothesis, we synthesized via ROMP four different amine telechelics comprising a predetermined amount of oxygen atoms in the polymer backbone. We found a direct relationship between the polarity of the polymer backbone and the ability of the BTA to form phase-segregated nanorods. We observed a decrease of the solid to isotropic phase transitions with increasing polarity. This phase transition is related to the loss of intermolecular hydrogen bonds as confirmed with IR and CD spectroscopy. Therefore, we can conclude that polarity effects are very important and play a key role in the formation and stabilization of BTA aggregates in dilute solution and in the solid state. This work adds to the understanding of hydrogen-bond engineering in supramolecular polymers.

Acknowledgment. We acknowledge M. M. E. Koenigs and J. Roosma for insightful discussions, A. J. H. Spiering for providing pTHF-bisamine, and M. A. J. Gillissen and D. J. G. Thielen for providing *N,N′*-(1,20-eicos-10-endiyl)-bis(isoindole-1,3-dione). This work is supported by the Council for Chemical Sciences of The Netherlands Organization for Scientific Research (NWO-CW).

Supporting Information Available: Fitting of temperature-dependent CD data; UV spectroscopy of (*R*)-**1** in MTBE (Figure S1); CD spectroscopy of (*R*)-**1** in MTBE (Figure S2); temperature-dependent CD data of (*R*)-**1** MTBE/MCH mixtures (Figure S3); DSC trace of polymer **4d** (Figure S4); solid-state infrared spectra of **4a**−**g** as a function of temperature (Figure S5). This material is available free of charge via the Internet at http://pubs.acs.org.

References and Notes

(1) Ciferri, A. *Supramolecular Polymers*; Marcel Dekker: New York, 2000.
(2) Lehn, J.-M. *Polym. Int.* **2002**, *51*, 825–839.
(3) Bosman, A. W.; Brunsveld, L.; Folmer, B. J. B.; Sijbesma, R. P.; Meijer, E. W. *Macromol. Symp.* **2003**, *201*, 143–154.
(4) Brunsveld, L.; Folmer, B. J. B.; Meijer, E. W.; Sijbesma, R. P. *Chem. Rev.* **2001**, *101*, 4071–4097.
(5) Ciferri, A. *Macromol. Rapid Commun.* **2002**, *23*, 511–529.
(6) Velten, U.; Rehahn, M. *Chem. Commun.* **1996**, 2639–2640.
(7) Hofmeier, H.; Hoogenboom, R.; Wouters, M. E. L.; Schubert, U. S. *J. Am. Chem. Soc.* **2005**, *127*, 2913–2921.
(8) Hilger, C.; Stadler, R. *Macromolecules* **1990**, *23*, 2095–7.
(9) de Greef, T. F. A.; Smulders, M. M. J.; Wolffs, M.; Schenning, A. P. H. J.; Sijbesma, R. P.; Meijer, E. W. *Chem. Rev.* **2009**, *109*, 5687–5754.
(10) van Beek, D. J. M.; Gillissen, M. A. J.; van As, B. A. C.; Palmans, A. R. A.; Sijbesma, R. P. *Macromolecules* **2007**, *40*, 6340–6348.
(11) Folmer, B. J. B.; Sijbesma, R. P.; Versteegen, R. M.; van der Rijt, J. A. J.; Meijer, E. W. *Adv. Mater.* **2000**, *12*, 874–878.
(12) Kautz, H.; van Beek, D. J. M.; Sijbesma, R. P.; Meijer, E. W. *Macromolecules* **2006**, *39*, 4265–4267.
(13) Colombani, O.; Barioz, C.; Bouteiller, L.; Chaneac, C.; Fomperie, L.; Lortie, F.; Montes, H. *Macromolecules* **2005**, *38*, 1752–1759.
(14) Dankers, P. Y. W.; Harmsen, M. C.; Brouwer, L. A.; van Luyn, M. J. A.; Meijer, E. W. *Nat. Mater.* **2005**, *4*, 568–74.
(15) Dankers, P. Y. W.; Meijer, E. W. *Bull. Chem. Soc. Jpn.* **2007**, *80*, 2047–2073.
(16) Wisse, E.; Renken, R. A. E.; Roosma, J. R.; Palmans, A. R. A.; Meijer, E. W. *Biomacromolecules* **2007**, *8*, 2739–2745.
(17) Wietor, J. L.; Sijbesma, R. P. *Angew. Chem., Int. Ed.* **2008**, *47*, 8161–8163.
(18) Bergman, S. D.; Wudl, F. *J. Mater. Chem.* **2008**, *18*, 41–62.
(19) Wool, R. P. *Soft Matter* **2008**, *4*, 400–418.
(20) Bosman, A. W.; Sijbesma, R. P.; Meijer, E. W. *Mater. Today* **2004**, *7*, 34–39.
(21) Hirst, A. R.; Escuder, B.; Miravet, J. F.; Smith, D K. *Angew. Chem., Int. Ed.* **2008**, *47*, 8002–8018.
(22) Hartgerink, J. D.; Beniash, E.; Stupp, S. I. *Science* **2001**, *294*, 1684–1688.
(23) Wu, D.; Pisula, W.; Enkelmann, V.; Feng, X.; Müllen, K. *J. Am. Chem. Soc.* **2009**, *131*, 9620–9621.
(24) Chen, Z.; Lohr, A.; Saha-Möller, C. R.; Würthner, F. *Chem. Soc. Rev.* **2009**, *38*, 564–584.
(25) Hill, J. P.; Jin, W.; Kosaka, A.; Fukushima, T.; Ichihara, H.; Shimomura, T.; Ito, K.; Hashizume, T.; Ishii, N.; Aida, T. *Science* **2004**, *304*, 1481–1483.
(26) Fox, J. D.; Rowan, S. J. *Macromolecules* **2009**, *42*, 6823–6835.
(27) Guan, Z.; Roland, J. T.; Bai, J. Z.; Ma, S. X.; McIntire, T. M.; Nguyen, M. *J. Am. Chem. Soc.* **2004**, *126*, 2058.
(28) Botterhuis, N. E.; Karthikeyan, S.; Veldman, D.; Meskers, S. C. J.; Sijbesma, R. P. *Chem. Commun.* **2008**, 3915–3917.
(29) Versteegen, R. M.; Sijbesma, R. P.; Meijer, E. W. *Macromolecules* **2005**, *38*, 3176–3184.
(30) Hirschberg, J. H.; Brunsveld, L.; Ramzi, A.; Vekemans, J. A. J. M.; Sijbesma, R. P.; Meijer, E. W. *Nature* **2000**, *407*, 167–70.
(31) Sijbesma, R. P.; Beijer, F. H.; Brunsveld, L.; Folmer, B. J. B.; Hirschberg, J. H. K. K.; Lange, R. F. M.; Lowe, J. K. L.; Meijer, E. W. *Science* **1997**, *278*, 1601–1604.
(32) Beijer, F. H.; Sijbesma, R. P.; Kooijman, H.; Spek, A. L.; Meijer, E. W. *J. Am. Chem. Soc.* **1998**, *120*, 6761–6769.
(33) Versteegen, R. M.; Kleppinger, R.; Sijbesma, R. P.; Meijer, E. W. *Macromolecules* **2006**, *39*, 772–783.
(34) Hirschberg, J. H. K. K.; Koevoets, R. A.; Sijbesma, R. P.; Meijer, E. W. *Chem.—Eur. J.* **2003**, *9*, 4222–4231.
(35) Whitesides, G. M.; Simanek, E. E.; Mathias, J. P.; Seto, C. T.; Chin, D.; Mammen, M.; Gordon, D. M. *Acc. Chem. Res.* **1995**, *28*, 37–44.
(36) Sivakova, S.; Bohnsack, D. A.; Mackay, M. E.; Suwanmala, P.; Rowan, S. J. *J. Am. Chem. Soc.* **2005**, *127*, 18202–18211.
(37) Botterhuis, N. E.; van Beek, D. J. M.; van Gemert, G. M. L.; Bosman, A. W.; Sijbesma, R. P. *J. Polym. Sci., Part A: Polym. Chem.* **2008**, *46*, 3877–3885.
(38) Roosma, J.; Mes, T.; Leclère, P.; Palmans, A. R. A.; Meijer, E. W. *J. Am. Chem. Soc.* **2008**, *130*, 1120–1121.
(39) Yasuda, Y.; Iishi, E.; Inada, H.; Shirota, Y. *Chem. Lett.* **1996**, 575–576.
(40) Hanabusa, K.; Kawakami, A.; Kimura, M.; Shirai, H. *Chem. Lett.* **1997**, 191–192.
(41) Sakamoto, A.; Ogata, D.; Shikata, T.; Hanabusa, K. *Macromolecules* **2005**, *38*, 8983–8986.
(42) Shikata, T.; Ogata, D.; Hanabusa, K. *J. Phys. Chem. B* **2004**, *108*, 508–514.

(43) de Loos, M.; van Esch, J. H.; Kellogg, R. M.; Feringa, B. L. *Tetrahedron* **2007**, *63*, 7285.
(44) Blomenhofer, M.; Ganzleben, S.; Hanft, D.; Schmidt, H.-W.; Kristiansen, M.; Smith, P.; Stoll, K.; Maeder, D.; Hoffmann, K. *Macromolecules* **2005**, *38*, 3688–3695.
(45) Mohmeyer, N.; Behrendt, N.; Zhang, X.; Smith, P.; Altstädt, V.; Sessler, G. M.; Schmidt, H.-W. *Polymer* **2007**, *48*, 1612.
(46) Lightfoot, M. P.; Mair, F. S.; Pritchard, R. G.; Warren, J. E. *Chem. Commun*. **1999**, 1945–1946.
(47) Brunsveld, L.; Schenning, A. P. H. J.; Broeren, M. A. C.; Janssen, H. M.; Vekemans, J. A. J. M.; Meijer, E. W. *Chem. Lett*. **2000**, 292–293.
(48) Smulders, M. M. J.; Schenning, A. P. H. J.; Meijer, E. W. *J. Am. Chem. Soc*. **2008**, *130*, 606–611.
(49) van Bommel, K. J. C.; van der Pol, C.; Muizebelt, I.; Friggeri, A.; Heeres, A.; Meetsma, A.; Feringa, B. L.; van Esch, J. *Angew. Chem., Int. Ed*. **2004**, *43*, 1663–1667.
(50) Obert, E.; Bellot, M.; Bouteiller, L.; Andrioletti, F.; Lehen-Ferrenbach, C.; Boue, F. *J. Am. Chem. Soc*. **2007**, *129*, 15601–15605.
(51) Stals, P. J. M.; Haveman, J. F.; Martín-Rapún, R.; Fitié, C. F. C.; Palmans, A. R. A.; Meijer, E. W. *J. Mater. Chem*. **2009**, *19*, 124–130.
(52) Scherman, O. A.; Ligthart, G. B. W. L.; Ohkawa, H.; Sijbesma, R. P.; Meijer, E. W. *Proc. Natl. Acad. Sci. U.S.A*. **2006**, *103*, 11850–11855.
(53) van Beek, D. J. M.; Spiering, A. J. H.; Peters, G. W. M.; te Nijenhuis, K.; Sijbesma, R. P. *Macromolecules* **2007**, *40*, 8464–8475.
(54) Stals, P. J. M.; Smulders, M. M. J.; Martín-Rapún, R.; Palmans, A. R. A.; Meijer, E. W. *Chem.—Eur. J*. **2009**, *15*, 2071–2080.
(55) Jonkheijm, P.; van der Schoot, P.; Schenning, A. P. H. J.; Meijer, E. W. *Science* **2006**, *313*, 80–83.
(56) Koevoets, R. A.; Versteegen, R. M.; Kooijman, H.; Spek, A. L.; Sijbesma, R. P.; Meijer, E. W. *J. Am. Chem. Soc*. **2005**, *127*, 2999–3003.
(57) Wisse, E.; Spiering, A. J. H.; van Leeuwen, E. N. M.; Renken, R. A. E.; Dankers, P. Y. W.; Brouwer, L. A.; Van Luyn, M. J. A.; Harmsen, M. C.; Sommerdijk, N. A. J. M.; Meijer, E. W. *Biomacromolecules* **2006**, *7*, 3385–3395.
(58) Grubbs, R. H. *Handbook of Metathesis*; Wiley-VCH: Weinheim, 2004.
(59) ROMP of cyclic olefins in the presence of a BTA-functionalized chain transfer agent did result in less control over the molecular weight and PDI.
(60) Hillmyer, M. A.; Grubbs, R. H. *Macromolecules* **1995**, *28*, 8662.
(61) Hrkach, J. S.; Matyjaszewski, K. *J. Polym. Sci., Part A: Polym. Chem*. **1995**, *33*, 285–298.
(62) The inability of the BTA motif to form helical structures when embedded in pCL was observed in earlier unpublished work.
(63) Pimentel, G. C.; McClellan, A. L. *The Hydrogen Bond*; W.H. Freeman and Co.: San Francisco, 1960.